Biophysical Chemistry, 48 (1993) 101–111
Elsevier Science Publishers B.V., Amsterdam

BIOCHE 01800

Femtosecond time-resolved fluorescence spectroscopy of bacteriorhodopsin: Direct observation of excited state dynamics in the primary step of the proton pump cycle

Mei Du and Graham R. Fleming *

Department of Chemistry and The James Franck Institute, The University of Chicago, 5735 S. Ellis Ave. Chicago, IL 60637 (USA)

(Received 13 May 1993; accepted in revised form 29 July 1993)

Abstract

A femtosecond fluorescence upconversion apparatus was used to measure the fluorescence decays in bacteriorhodopsin from *Halobacterium halobium*. The isotropic fluorescence measurements reveal a weak emission wavelength dependence from 680 nm to 900 nm (which spans most of the steady state fluorescence spectrum). The decays can be well fitted as a sum of three exponential decay components with time constants in the range of 90 fs–240 fs, 0.6 ps–0.9 ps, and 9.0–13.0 ps. We discuss the mechanism for non-exponentiality in terms of the intrinsic characteristics of a barrierless reaction and/or the distribution of parameters affecting the reactive process. We discuss the kinetics by comparing with previous pump-probe transient absorption measurements, and suggest that the first time constant results from either a relaxation process in the first singlet excited state of the retinal molecule or from the reactive process from the excited state to the photoproduct and reactant. We associate the longer components solely with the reactive process from the excited state to the photoproduct and ground state of bacteriorhodopsin. Fluorescence depolarization measurements reveal a wavelength dependent initial anisotropy. The fluorescence data do not seem to be easily explainable with a one-dimensional potential surface model.

Keywords: Bacteriorhodopsin; Femtosecond time-resolved fluorescence; Proton pump photoisomerization; Emission/excited state dynamics; Spontaneous emission

1. Introduction

Bacteriorhodopsin (BR) is a protein in the purple membrane of *Halobacterium halobium* that is responsible for the conversion of light energy to electrochemical energy by the generation of a transmembrane proton gradient [1]. Light absorbed by the retinal molecule bacteriorhodopsin initiates a reaction cycle of the retinal molecule and the protein moiety, which involves several intermediates distinguishable through their absorption spectra [2–5]. Extensive studies suggest that the intermediates arise from conformational changes of the retinal molecule and/or the protein and from deprotonation/reprotonation of the Schiff base and adjacent amino acids [2–5]. Changes of retinal chromophore geometry and protonation state of amino acid residuals during the photocycle were identified by spectroscopic

* Corresponding author.

measurements in bacteriorhodopsin [2–5]. The light-induced primary step to form intermediate K of this cycle is ultrafast (timescale of a few picoseconds) and efficient compared to other energy dissipation processes and results in about 16 kcal/mol being stored in intermediate K [6] to facilitate subsequent thermal relaxation in completing the proton pump cycle. The quantum yield for isomerization has been previously reported to be in the range from 0.25 [7] to 0.79 [8] with the remainder of the retinal molecules returning to the initial all-trans configuration of BR. Very recently, Rohr et al reported a quantum yield of 0.6 measured via femto- and nanosecond optoacoustic spectroscopy [9].

Bacteriorhodopsin is the simplest and best understood active transport system. It thus provides an excellent system to explore a biological reaction mechanism from the perspective of chemical physics [2–5,10–24]. Many studies has been devoted to the mechanism of the primary step in the proton pump cycle [3–5,10–24], i.e. the dynamics of and structural changes accompanying the formation of the first intermediate, K, which can be trapped. Resonance Raman [19–22] led to the conclusion that the first step is the photoisomerization of the retinal chromophore (BR) and K is the distorted 13-*cis* configuration. The retinal chromophore, initially in the all trans configuration, undergoes a torsional isomerization around the C_{13}=C_{14} double bond following excitation to the first excited state S1 and undergoes a non-radiative transition to form the 13-*cis* photoproduct [2–5,10–24]. Previous time-resolved optical measurements have shown that the isomerized photoproduct, J, characterized by a red-shifted absorption spectrum, appears within 500 fs [4,5,10–17]. Subsequently, the intermediate K is formed on a 3 ps time scale [4,5,11,12,14–16].

Temperature-dependent experiments showed that the K intermediate is formed even at 1.5 K [18]. The rest of the photo cycle can be stopped by lowering the temperature and is considered to be thermally activated [5]. The kinetics of the primary step, as well as the wavelength and temperature independence of the quantum efficiency suggest a barrierless excited state reaction to form the primary photoproduct [25]. Sundstrom and coworkers have discussed the primary step as an example of a barrierless reaction [25].

As is common in natural photosynthetic systems, bacteriorhodopsin has a broad and structureless absorption spectrum, the absorption spectra of the intermediates overlap strongly and the excited state absorption spectrum is very broad. These highly congested spectra for both reactant (BR) and products (J,K,L,M,N,O,..) complicate dynamics studies using transient absorption measurements. As a complementary approach, time-resolved fluorescence measurements enable direct observation of the excited state dynamics, free of excited state or photoproduct absorption. In this paper, we report a time-resolved fluorescence study of BR which in combination with transient absorption data should provide more information on the molecular dynamics of the primary step of the BR cycle.

The observation by Lewis et al. [26] of light emission from bacteriorhodopsin has opened up the possibility of using fluorescence studies to learn more about the primary step in bacteriorhodopsin energy conversion process. Previous fluorescence measurements gave differing results. Alfano and coworkers reported a 3 ps decay time for the first excited state of BR using the fluorescence Kerr gate technique [27], Hirsch and coworkers reported a 15 ps decay time constant using the fluorescence upconversion technique [28]; and Shapiro and coworkers obtained 60 ± 15 ps at 77 K using a streak camera [29]. The quantum efficiency for emission is reported to be $(2.4–10) \times 10^{-5}$ [30]. An estimate of the radiative rate from the absorption spectrum gives $(6\ \text{ns})^{-1}$ [30], leading to an estimate of 0.14 ps–0.6 ps for the fluorescence lifetime. Obviously, adequate time resolution is required to resolve the BR excited state dynamics. Here we used the fluorescence upconversion technique with a time resolution of about 40 fs. The isotropic fluorescence decays were measured from 680 nm to 900 nm, a wavelength range which spans most of the steady state fluorescence spectrum [12]. Fluorescence depolarization was also measured at a range of wavelengths in an attempt to follow the geometry changes of the retinal molecule. The isotropic fluorescence decays and fluorescence depolariza-

tion are presented in Section 3. In Section 4, we discuss the molecular mechanism of the primary step of the BR proton pump cycle.

2. Experimental

Fluorescence measurements were performed by the upconversion technique, which we believe provides the best approach when femtosecond time resolution is required. The fluorescence upconversion apparatus is based on a cavity-dumped antiresonant ring dye laser. Typically this laser provides pulses shorter than 75 fs FWHM with 2–3 nJ pulse energy. Amplification of single pulse of the dye laser is achieved by using a two-stage single pass dye amplifier pumped by the frequency doubled output of regenerative amplifier [31]. The amplified output pulses, centered at 608 nm have an average energy of ~240 nJ at a repetition rate of 100 kHz. Compensation for the group velocity dispersion is made using a pair of SF-10 prisms in a near-retroreflecting geometry. Half of the pulse is reflected and directed to the mixing crystal as the gate pulse, the remaining half is filtered to reduce the intensity and used as the excitation pulse. The experimental setup is shown in Fig. 1. The essential improvement from an earlier design [32,33] is in the optics for collecting fluorescence. We used an elliptical reflector rather than the Cassegranian arrangement used by Shah [32] and Mokhtari and coworkers [33]. The elliptical reflector is positioned such

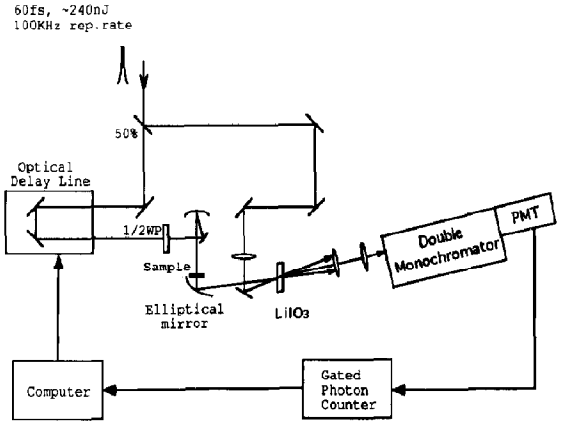

Fig. 1. Fluorescence upconversion apparatus.

that the sample is at the first focus and the mixing crystal, in our case a 400 μm thick $LiIO_3$ crystal, is at the second focus. The fluorescence is mixed with the gate pulse in a near-collinear geometry. The excitation pulse is centered at 608 nm and has 3 nJ of energy per pulse, while the gate pulse, also centered at 608 nm, has 10 nJ of energy per pulse. The upconverted UV signal is directed to an Instruments SA DH-20 double monochromator using careful mode matching. The spectrally selected UV signal is then detected by a PMT, and recorded by a Stanford Research Systems model 400 photon counter. Typical pump-gate cross correlation functions had a FWHM of 60–70 fs. The stability of the laser is monitored by detecting a small portion of the excitation beam by a PMT and sampling it with a Boxcar. The intensity fluctuation was within a few percent, hence normalization of the raw data was not employed. The stability of the laser and the sensitivity of the detection system make it possible to detect the signal close to the photon noise background. In our measurements, the count rate at the peak of the decay is 30–70 per second, depending on the wavelength and polarization detected. 10–15 scans were added to give one decay curve.

Fluorescence decay curves were recorded with the polarization of the excitation pulse parallel, perpendicular or at the magic angle (54.7°) relative to the polarization of the gate pulse to obtain $I_{\parallel}(t)$, $I_{\perp}(t)$ and $I_{\mathrm{iso}}(t)$. The anisotropy decay $r(t)$ and isotropic decay $K(t)$ are related to the parallel and perpendicular fluorescence curves by

$$r(t) = \left[I_{\parallel}(t) - I_{\perp}(t)\right] / \left[I_{\parallel}(t) + 2I_{\perp}(t)\right] \quad (1)$$

$$K(t) = I_{\mathrm{iso}}(t) = I_{\parallel}(t) + 2I_{\perp}(t) \quad (2)$$

The measured parallel and perpendicular data were analyzed by simultaneous iterative reconvolution and nonlinear least-squares fitting of both data sets as described by Cross and Fleming [34]. The measured isotropic data were analyzed using the MINUIT package, and the fitted results, in turn, were used as the boundaries for anisotropy analysis. The instrument response function used in fitting was taken to have a similar shape to the measured cross correlation function but to be 20–60 fs broader to take into account the group

velocity mismatch between the fluorescence and the gate pulse [32]. The amount of broadening varies with the detected fluorescence wavelength.

Care has been taken to assure accurate depolarization measurements. No polarizer is used after the sample in order to maintain high time resolution and sensitivity. First, a clean S-polarized mixing beam and careful alignment of the $LiIO_3$ crystal assures that only the S-polarized fluorescence is upconverted. Second, the solid angle of the fluorescence collection was reduced by masking the elliptical mirror except for a narrow strip in the plane of the laser beams on one half of the elliptical mirror in order to prevent scrambling of the S- and P-polarization by the mirror. We verified the initial anisotropy of cresyl violet in ethanol is 0.40 ± 0.02. Finally, the parallel and perpendicular fluorescence signals were obtained by rotating the polarization of the excitation beam, such that the upconverted UV signal detected by monochromator and PMT has the same polarization for both parallel and perpendicular signals. The scans were taken alternately for parallel and perpendicular polarizations to minimize the influence of any long term laser drift and possible sample degradation.

Bacteriorhodopsin was purchased from Sigma. A suspension was prepared with distilled water, sonicated in ice for 5 seconds and then let to rest for 10 seconds in ice to avoid thermal heating of the sample. All measurements were carried out at room temperature. The absorption spectrum was used to monitor the sample, which showed an absorption maximum at 568 nm and no detectable change during the measurements. The optical density of the sample in a 1 mm cell was 0.38 at 610 nm. The sample was stirred at about 20 Hz during the measurements by a filament attached to an electric tooth brush. Light adaptation, which maintains the chromophore in its active conformation, was ensured by continuous background illumination using a light bulb.

3. Results

Earlier fluorescence studies concluded that the emission emanates from the excited state of a single species [26,30], i.e. intermediates do not emit in the steady state fluorescence spectral region. Short decay components and no detectable rising components in our results presented in this section also rule out that intermediates J, K, L, M, N, O, etc., are the fluorescing species, which is consistent with the previous conclusions [5,6,26,30] that all intermediates are formed in their ground electronic states. On the other hand, we should consider the possible effects of building up a steady state concentration of intermediates. Our high repetition rate and low stirring rate may not be sufficient to remove the sample from the pump focal volume. This may allow subsequent excitation pulses to interact with intermediates in the photocycle which the proceeding pulse initiated. We estimate that the contribution of this emission to the signal is less than 5% and we will neglect this artifact in the following discussion.

3.1. Isotropic fluorescence measurements

Figure 2 shows typical fluorescence signals at 770 nm emission recorded over 2 ps, 5 ps and 30 ps scans. The decays were fitted to a sum of exponentials convoluted with the instrument response function. The instrument response function was determined by the cross correlation of the pump pulse and gate pulse corrected by the group velocity mismatch [32]. The signal cannot be fitted by single exponential or sum of two exponentials, but a sum of three exponentials gives a good fits to the fluorescence signals. An iterative fitting procedure using three different scan lengths was used to determine the widely separated time constants. A 30 ps scan was used to determine the longest time constant, which was then used as a constraint in a fit of the 5 ps data for the intermediate time constant. Finally the longest and intermediate time constants were used to obtain the shortest time constant from a 2 ps scan. This iterative procedure was essential because of the wide separation of the three time constants.

Three characteristics of the decays can be listed. (1) Three time constants are required to fit the data at all wavelengths. They are 90 fs–240 fs

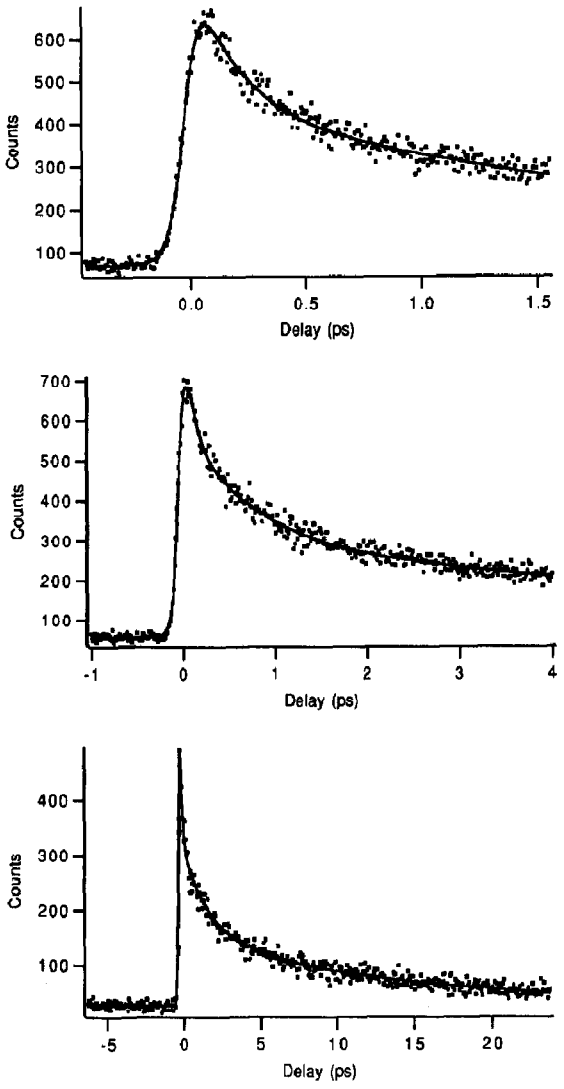

Fig. 2. Typical fluorescence decays detected at 770 nm at different scan length.

with 40–70% amplitude, 0.6 ps–0.9 ps with 20–40% amplitude, and 8–13 ps with 5–25%. amplitude. Values of three parameters as a function of emission wavelength are given in Table 1. (2) With our current time resolution, uncertainty in determining the group velocity mismatch, and signal-to-noise ratio, there is no detectable rise time at any wavelength detected. (3) The fluorescence decays are slightly dependent on emission wavelength over 3380 cm^{-1} spectral detection region. The overall decay rate decreases as emission wavelength increases from 680 nm to 800 nm

Table 1

Best fits at 608 nm excitation [a]

Emission Wavelength (nm)	a_1 (%)	τ_1 (ps)	a_2 (%)	τ_2 (ps)	a_3 (%)	τ_3 (ps)
680	68	0.090	25	0.68	7	xx
690	64	0.098	30	0.67	6	10.9
700	61	0.10	34	0.72	5	9.8
720	50	0.14	43	0.76	8	xx
750	47	0.14	42	0.82	11	xx
770	41	0.17	32	0.75	27	10.3
800	51	0.20	23	0.80	25	8.9
830	53	0.22	33	0.80	14	10.4
870	55	0.20	32	0.78	13	10.8
900	56	0.24	25	0.80	19	12.8

[a] Standard deviations were determined to be 0.05 ps, 0.15 ps and 3.0 ps for three time constant respectively. xx represents parameters which could not be determined because of the lack of a longer scan.

and increases slightly from 800 nm to 900 nm, i.e. the overall decay rate is smaller near 800 nm. Fluorescence decays at several emission wavelengths are shown in Fig. 3.

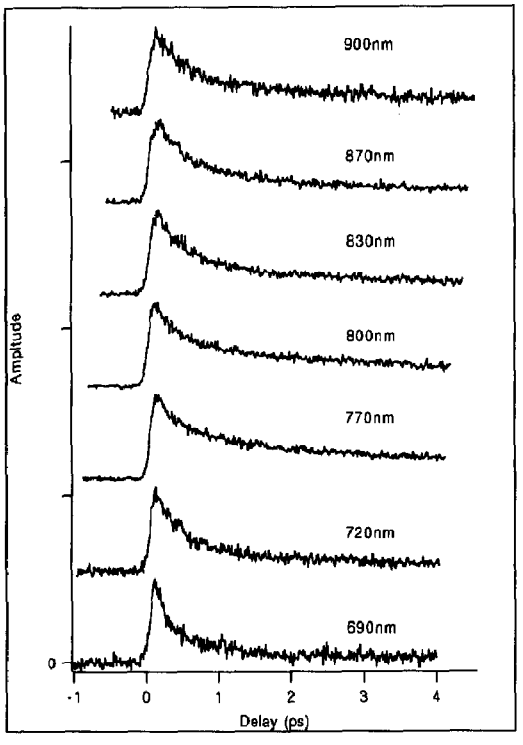

Fig. 3. Fluorescence decays at different detection wavelengths measured over 5 ps scan length.

3.2. Fluorescence depolarization measurements

Fluorescence anisotropy decay curves were measured at three different detection wavelengths, i.e. at 700 nm (on the blue side of the steady state fluorescence spectrum), 800 nm (on the red side of the spectrum), and 900 nm (in the red tail of the spectrum). Figure 4 shows a typical data set recorded with 608 nm excitation and 700 nm emission detected with a 4 nm bandwidth. A fit including convolution with the instrument response function (100 fs) gives an initial anisotropy of 0.35 ± 0.04. Figure 5 shows a fluorescence data set at 800 nm emission wavelength. An analysis of the data gives an initial anisotropy 0.25 ± 0.04 and no anisotropic decay in the scan time region (2 ps). A similar result was found for fluorescence detected at 900 nm, which gave an initial anisotropy of 0.26, and no anisotropic decay up to 2 ps.

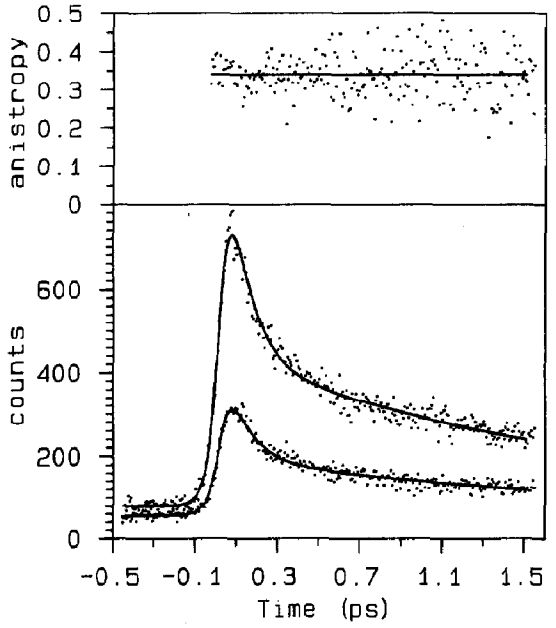

Fig. 4. Fluorescence depolarization data set measured at 700 nm. The solid lines are fitted curves and the dots represent data. Upper panel: Raw anisotropy (dots) and the fit (solid line) R(0) = 0.35. Lower panel: Parallel (upper) and perpendicular (lower) data and fits.

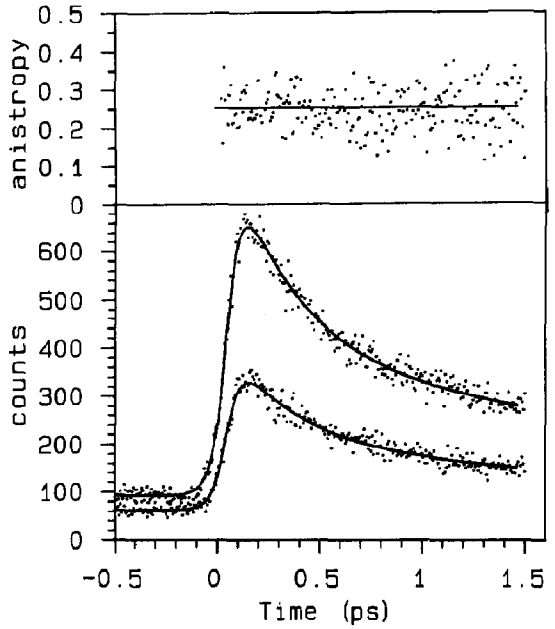

Fig. 5. Similar data as Fig. 4 measured at 800 nm.

3.3. Spectral evolution

Time-resolved fluorescence spectra were obtained using the methods described by Maroncelli and Fleming [35]. The time resolved spectra show an amplitude decrease as a function of time with slight changes in peak position, spectral width, and shape with time up to 5 ps (not shown).

4. Discussion

Both the relevant potential surfaces of bacteriorhodopsin and the dynamics thereon may be very complex. Even on a simple one-dimensional harmonic surface, barrierless reactions can lead to highly non-exponential population kinetics [25,36–38]. It has been noted that fluorescence decay, excited state absorption and ground state recovery measurements may show differing time-dependence in such cases [37]. The case of complex potential surfaces in which the reaction coordinate (which in this case is considered to be the C_{13}–C_{14} torsional angle) is coupled to a large number of other degrees of freedom, many of which may have sizable displacements from the

ground state minimum [21], further complicates the interpretation. For guidance on the features of such a system we turn to the molecular dynamics simulations of Warshel et al. on bacteriorhodopsin [23]. These authors conclude that torsional energy rapidly relaxes into other degrees of freedom and thus damped rather than free (inertial) motion on the excited state surface is appropriate. They consider that the most likely potential surface has the ground state maximum coinciding with the excited state minimum along the torsional coordinate, and the time required to reach the twisted excited state from the Franck–Condon geometry is about 200 fs. In the following, we discuss the implications of our experimental results in terms of mechanisms for non-exponentiality, dynamics of the primary step, and the influence of protein in combination with previous experimental results and molecular dynamics simulation.

Three mechanisms might be responsible for non-exponentiality: (1) intrinsic characteristics of a barrierless process, (2) a distribution in parameters influencing the reactive process, and (3) chromophore and/or protein relaxation on the reaction time scale. In general, time-resolved fluorescence measurements probe the population change within a narrow spectral window. In an isomerization process, the dynamics of population relaxation on the excited state potential surface could result from motion out of the Franck–Condon region towards an efficient sink and/or decay of population from the sink to partition between product(s) and reactant. In this context, the BR system resembles *cis*-stilbene where this point has been recently discussed in some detail [39–42]. However, fluorescence decays for *cis*-stilbene are well described as single exponential, in sharp contrast with the bacteriorhodopsin decays measured here.

The notion that proteins may exist in many conformational substates has been discussed in detail by Frauenfelder and coworkers [43]. Bacteriorhodopsin is located in a protein pocket and the potential surface along the reaction coordinate and therefore the energy separation between excited and ground states are expected to depend on the conformation of the protein pocket and the interaction between the chromophore and its protein environment. The probability of the nonadiabatic transition to the ground state will generally depend exponentially on the energy gap ΔE via $P(E) = \exp(-\gamma \Delta E)$ [36]. Resonance Raman spectroscopy [21] and photochemical hole burning [18], give an inhomogeneous broadening for the absorption spectrum of about 1100 cm^{-1} at room temperature and ~ 470 cm^{-1} at 1.5 K. In their molecular dynamics simulation Warshel et al. [23] found that when the excited state potential was flattened so that the twisted minimum was 10 kcal/mol below the potential of the planar trans form rather than ~ 22 kcal/mol as in the initial simulation, the time taken to reach the twisted region increased from 200 fs to 600 fs. A distribution of twisting times combined with a distribution of nonadiabatic relaxation rates from the twisted state could clearly be responsible for the non-exponential kinetics. In this context it will be interesting to compare solution studies with the protein studies. A recent fluorescence upconversion study of the protonated Schiff base in methanol finds single exponential decay on both the blue and red side of the spectrum with time constants of 90 fs and 3.7 ps, respectively [44]. In the center of the spectrum the decay is non-exponential and components of 500 fs and 2.8 ps were obtained [44].

Chromophore and protein relaxation on the time scale of the reactive process may also lead to a time-dependent fluorescence spectrum, which would then give non-exponential decays in a given detection window. The data in Table 1 indicate that kinetics vary slightly across the steady state fluorescence spectrum and our calculation on the time-resolved fluorescence spectra show that the spectral evolution is small. Thus this mechanism will not cause a large deviation from exponential decay.

In the context of a model involving a large angle twist in a few hundred femtoseconds, the lack of a substantial red shift in the spectrum may seem surprising. However, the optical transition in BR is coupled to a large number (29) of modes many of which have substantial displacements from the ground state [21]. The type of spectrum we observe and the trends in the decay curves

shown in Fig. 3 are qualitatively consistent with expectations based on a model in which those modes which are prepared in eigenstates (i.e. are of too high frequency to be impulsively excited) have much smaller displacements from their equilibrium values near the twisted configuration and follow the twisting motion adiabatically. The requirement that excitation is not impulsive with respect to the displaced modes is imposed both by the lack of any rise time in our signals, even for shifts as large as 5556 cm^{-1}, and the wavelength dependence of the initial anisotropy. The slightly faster overall decays on both the blue and red side of the spectrum as compared with the center of the spectrum in Fig. 3 are consistent with a slight narrowing of the emission spectrum as the displacements of the high frequency modes decrease along the twisting coordinate. In this model, our wavelength dependent initial anisotropy is not unreasonable. The Franck–Condon active high frequency modes, which are adiabatically coupled to the reaction coordinate, could sample different electronic character of the transition at different displacements in the high frequency modes in the states involved in the emission on the time scale of the vibrational period of high frequency modes. In this picture, the final states reached by emission are at different locations orthogonal to the reaction coordinate and give different initial anisotropy within our time resolution.

In order to set our results in context, we next provide a brief summary of the results of pump-probe spectroscopy on this system. In transient absorption spectroscopy, ground state recovery, excited state absorption and stimulated emission can all be measured separately [4,5,10–17]. When the probe is at 568 nm, transient absorption experiments with a time resolution of 12 fs [17], find little change in the probe transmission until approximately 200 fs This observation suggests a delay in the ground state recovery. Two obvious possibilities can be considered for this delay: relaxation in the excited state [10–17] and/or the vibrational relaxation in the ground state. The available data support the first mechanism [10–17]. In addition, the ground state was observed to recover with a characteristic time ~ 430 fs–530 fs in transient pump-probe experiments at 560–600 nm [10–17].

When probe wavelength is tuned to the fluorescence spectrum region, stimulated emission revealed various decay components across the steady state fluorescence spectrum [10–12]. Dobler et al. reported stimulated emission from 695 nm to 930 nm, which showed a strong wavelength dependence. An approximately 200 fs decay component was observed at 695 nm and 735 nm detection, both 200 fs and 500 fs decay components were found at 850 nm and a 500 fs decay component was obtained at 930 nm [12]. These time constants set a lower limit for the excited state decay. The apparent inconsistency between stimulated emission and spontaneous emission may result from other contributions (e.g. photoproduct absorption) to the stimulated emission signal which suppress the longer components.

As the probe wavelength is tuned to 460 nm, the excited state absorption is measured and showed two decay components with time constants of 530 fs and 3200 fs [14–17]. The signals relating to the appearance of photoproducts are more complicated. In particular, the initial step of the intermediate J appearance is difficult to probe directly because of the spectral overlap of stimulated emission and the photoproduct absorption. Data collected in the photoproduct absorption region from 620 nm to 650 nm gave components of 450 fs and 5 ps [10–17].

The longest time constant ~ 10 ps in our fluorescence decays has not been reported from stimulated emission measurements, but was reported in earlier spontaneous emission (fluorescence) measurements [27,28] and in low pH conditions [40].

Dobler et al. [12] assign the 200 fs component to relaxation in the excited state and the 500 fs component to reaction to photoproduct and reactant, i.e. decay at the "sink", based on their wavelength dependent stimulated emission data. Following on the remarks at the beginning of this section, however, it is not clear that a specific meaning can be attached to the time constants obtained in the fits to the sum of exponentials. It does appear likely that a few hundred femtosecond "induction period" does exist before popula-

tion begins to leave the excited state surface. The ground state recovery signals are also complicated by the possibility of slow vibrational relaxation in the ground state. Very recently, resonance Raman experiments have been interpreted to suggest that J is a thermally unrelaxed or "hot" vibrational state and the J to K process corresponds to vibrational relaxation with a 3 ps time constant [22]. This implies a relatively long vibrational relaxation time even in the reaction coordinate. Pump-probe experiments with high time-resolution observed vibrational coherences for high frequency vibrational modes in ground state recovery persisting until 3 ps [17]. However, the simplest explanation for the 500 fs component observed in fluorescence, ground state recovery and excited state absorption is to associate it with the nonradiative process from the excited to ground state surfaces.

The longest component has been reported earlier with picosecond spectroscopy. About 15 ps for fluorescence lifetime [27,28] and 11 ps for intermediate K appearance [4,5] have been reported with picosecond resolution. The origin for the slowest component ~ 10 ps in fluorescence decay may result from inhomogeneity or intrinsic non-exponential kinetics or both.

In a number of respects BR resembles *cis*-stilbene whose isomerization has been studied extensively in solution [39–42] and in the gas phase by Greene and Farrow [46]. In both cases the absorption and emission spectra are broad and structureless. There is a large Stokes shift $-10{,}000\ \mathrm{cm}^{-1}$ for *cis*-stilbene and $5000\ \mathrm{cm}^{-1}$ for BR, but no detectable rise in the fluorescence signal for either *cis*-stilbene or BR. However, there are also some striking differences between the two systems. The isomerization is ultrafast with a range of time constants (see Table 1) in BR and 0.4 to 1.7 ps depending on solvent polarity and viscosity in *cis*-stilbene [40]. The decay of excited *cis*-stilbene is generally found to fit well to a single exponential time constant. (an exception is the fluorescence decay in decanol [40]). The ground state *trans*-stilbene product appears with a time constant indistinguishable from both the fluorescence decay and the excited state absorption [39,40]. By contrast the fluorescence decay of BR is highly non-exponential and differs substantially from the kinetics observed in transient absorption studies [10,12]. It is tempting to suggest that these differences arise from the BR binding site. The friction for the BR isomerization arises from internal coupling to non-reactive degrees of freedom and from electrostatic interaction and/or hydrogen bonding, rather than mechanical friction arising from collisions with solvent molecules. The extremely rapid isomerization in BR (cf. the 320 fs found for *cis*-trans photoisomerization of stilbene in the gas phase) suggests the process is essentially free from external friction.

The protein exerts a strong influence on the spectrum of the retinal molecule. The absorption spectrum maximum (λ_{max}) of the chromophore in BR is red-shifted by $5100\ \mathrm{cm}^{-1}$ from the λ_{max} of the chloride salt of the protonated Schiff base in methanol solution. This opsin shift results from changes in the retinal structure and environment caused by interaction with protein [47]. In addition, the quantum yield for the isomerization is increased from 0.2 in solution [47] to 0.6 in protein [9].

The Stark effect and two-photon resonance absorption give a dipole moment change from the ground state to the first excited state of 12.4 D and 13.5 D $\pm$ 0.8 D [48], respectively. Such a change is large compared to many dye molecules where large Stokes shifts are observed in polar liquids, yet no detectable red-shift in the BR fluorescence occurs. Similar behavior is found in the bacterial photosynthetic reaction center [49]. In BR the protein pocket is relatively rigid compared to liquid solvent and reconstruction of the local configuration is not to be expected on short time scales. A rapid dielectric relaxation of the protein has been found in computer simulations of the bacterial reaction center with a time constant of 100 fs [50]. Protein relaxation does, however, play an important role on the longer time scales in facilitating the proton pump cycle [4,5].

5. Summary

Spontaneous emission decays of bacteriorhodopsin were recorded using the fluorescence up-

conversion technique. Fluorescence decays over 680 nm–900 nm spectral region show weak wavelength dependence and are highly non-exponential. The initial fluorescence anisotropy varies with wavelength. We discuss our data in the context of a model in which high frequency modes, which are known to have large displacements at the *trans*-geometry, have much smaller displacements toward the twisted geometry. Our data are consistent with, but do not require, a model in which a relaxation process of 100–200 fs occurs on the excited state prior to electronic relaxation to the ground state surface and branching to initial and product geometries.

Acknowledgements

We thank Drs. David Jonas and Hideki Kandori for insightful discussion, Dr. David Jonas for comments on the manuscript, Dr. Sunney Xie for experimental assistance and Dr. Linda Peteanu for advice on sample preparation. We also thank Dr. Hideki Kandori for sending us ref. [15]. This research was supported by NSF grant CHE-9200588.

References

1 D. Oesterhelt and W. Stoeckenius, Proc. Natl. Acad. Sci. USA 70 (1973) 2853.
2 R. Henderson, J.M. Baldwin, T.A. Ceska, F. Zemlin, E. Beckmann and K.H. Dowwning, J. Mol. Biol. 213 (1990) 899.
3 W. Stoeckenius and R.A. Bogomolni, Annu. Rev. Biochem. 52 (1982) 587.
4 R.A. Mathies, S.W. Lin, J.B. Ames, and W.T. Pollard, Annu. Rev. Biophys. Chem. 20 (1991) 491.
5 R.R. Birge, Biochem. Biophys. Acta 1016 (1990) 293.
6 R.R. Birge and T.M. Cooper, Biophys. J 42 (1983) 61.
7 C.R. Goldschmidt, O. Kalisky, T. Rosenfeld and M. Ottolenghi, Biophys. J. 17 (1977) 179.
8 D. Oesterhelt and B. Hess, Eur. J. Biochem. 37 (1973) 316.
9 M. Rohr, W. Gartner, G. Schweitzer, A.R. Holzwarth and S.E. Braslavsky, J. Phys. Chem. 96 (1992) 6055.
10 R.A. Mathies, C.H. Brito Cruz, W.T. Pollard and C.V. Shank Science 240 (1988) 777.
11 M.C. Nuss, W. Zinth, W. Kaiser, E. Kolling and D. Oesterhelt, Chem. Phys. Left. 117 (1985) 1.
12 J. Dobler, W. Zinth, W. Kaiser and D. Oesterhelt, Chem. Phys. Lett. 144 (1988) 215.
13 W.T. Pollard, C.H. Brito Cruz, C.V. Shank and R.A. Mathies, J. Chem. Phys. 90 (1989) 199.
14 A. Sharkov, A. Pakulev, S. Chekalin and Y. Matveetz, Biochim. Biophys. Acta 808 (1985) 94.
15 H. Kandori, K. Yoshihara, H. Tomioka, H. Sasabe and Y. Shichida Chem. Phys. Lett. 211 (1993) 385.
16 J.W. Petrich, J. Breton, J.L. Martin and A. Antonetti, Chem. Phys. Lett. 137 (1987) 369.
17 S.L. Dexheimer, Q. Wang, L.A. Peteanu, W.T. Pollard, R.A. Mathies and C.V. Shank, Chem. Phys. Lett. 188 (1992) 61.
18 G.R. Loppnow, R.A. Mathies, T.R. Middendorf, D.S. Gottfried and S.G. Boxer, J. Phys. Chem. 96 (1992) 737.
19 R. Van den Berg, D. Jang, H.C. Bifting and M.A. El-Sayed, Biophys. J. 58 (1990) 135.
20 R. Lohrmann, I. Grieger and M. Stockburger, J. Phys. Chem. 95 (1991) 1993.
21 A. Myers, R. Harris and R. Mathies, J. Chem. Phys. 79 (1983) 603.
22 G.H. Atkinson, D. Blanchand, H. Lemaire, T.L. Brack and Hayashi, Biophys. J. 55 (1989) 263.
23 A. Warshel, Z.T. Chu and J.K. Hwang, Chem. Phys. 158 (1990) 303.
24 G.H. Atkinson, D. Blanchard and T.L. Brack, J. Luminescence 48 (1991) 410.
25 V. Sundstrom and U. Aberg, J. Mol. Liq. (1993) in press.
26 A. Lewis, J.P. Spoonhower and G.J. Perreault, Nature 260 (1976) 675.
27 R.R. Alfano, W. Yu, R. Govindjee, B. Becher and T.G. Ebrey, Biophys. J. 16 (1976) 541.
28 M.D. Hirsch, M.A. Marcus, A. Lewis, H. Mahr and N. Frigo, Biophys. J. 16 (1976) 1399.
29 S.L. Shapiro, A.J. Campillo, A. Lewis, G.J. Perreault, J.P. Spoonhower and R.K. Clayton, Biophys. J. 23 (1978) 383.
30 R. Govindjee, B. Becher and T.G. Ebrey, Biophys. J. 22 (1978) 67.
31 A. Ruggiero, N. Scherer, G. Mitchell, G. Fleming and J. Hogan, J. Opt. Soc. Am. B8 (1991) 2061.
32 J. Shah, IEEE S. Quantum Electronics 24 (1988) 276.
33 A. Mokhtari, A. Chebira and J. Chesnoy, J. Opt. Soc. Am. B7 (1990) 1551.
34 A. Cross and G. Fleming, Biophys. J. 46 (1984) 45.
35 M. Maroncelli and G.R. Fleming, J. Chem. Phys. 86 (1987) 6221.
36 B. Bagchi and G. Fleming, J. Phys. Chem. 94 (1990) 9.
37 B. Bagchi, U. Abery and V. Sundstrom, Chem. Phys. Lett. 162 (1989) 227.
38 J. Jean, G.R. Fleming and R.A. Friesner, Ber. Bunsenges. Phys. Chem. 95 (1991) 253.
39 R.J. Sension, A.Z. Szaka and R.M. Hochstrasser, J. Chem. Phys. 97 (1992) 5239.
40 D.C. Todd, J.M. Jean, S.J. Rosenthal, A.J. Ruggiero, D. Yang and G.R. Fleming, J. Chem. Phys. 93 (1990) 8658.
41 D.C. Todd and G.R. Fleming, J. Chem. Phys. 98 (1993) 269.

42 D.C. Todd, G.R. Fleming and J.M. Jean, J. Chem. Phys. 97 (1992) 8915.
43 H. Frauenfelder, F. Parak and R.D. Young, Annu. Rev. Biophys. Chem. 17 (1988) 451.
44 H.Kandori, Personal communication, 1993.
45 T. Kobayashi, H. Ohtani, J. Iwai, A. Ikegami and H. Uchiki, FEBS Lett. 162 (1983) 197.
46 B.I. Greene and R.C. Farrow, J. Chem. Phys. 78 (1983) 3336.
47 K. Nakanishi, V. Balogh-Nair, M. Arnaboldi, K. Tsujimoto and Honig, J. Am. Chem. Soc. 102 (1980) 7945.
48 R.R. Birge and C. Zhang, J. Chem. Phys. 92 (1990) 7178.
49 M. Du, S. Rothenthal, X. Xie, T. DiMagno, M. Schmit, J. Norris and G. Fleming, Proc. Natl. Acad. Sci. USA 89 (1992) 8517.
50 K. Shulten and M. Tessch, Chem. Phys. 158 (1991) 421.